Sequential oxidations of phenylchalcogenides by H₂O₂: insights in the redox behavior of selenium from a DFT analysis

Marco Bortoli,[a†] Matteo Bruschi, [a,b†] Marcel Swart[b,c]* and Laura Orian [a]*

The biological activity of sulfur and selenium, despite their similarity, shows some remarkable differences that have been recognized in many different scenarios. However, the underlying cause has not been completely clarified yet. The difference in redox behavior of these two chalcogens has lately been addressed as justification of the presence of selenium in some essential biological systems. In particular, selenium is found in some peroxidases, i.e. glutathione peroxidases (GPx), whose redox activity relies on a fast-reacting selenocysteine and is fundamental to metabolize harmful peroxides. In this work, a systematic *in silico* investigation on model systems, i.e. phenylchalcogenides, containing sulfur, selenium and tellurium is presented. Sequential oxidation reactions of these chalcogen-based substrates by hydrogen peroxide are carried out spanning the range of the biologically relevant chalcogen oxidation numbers [*Advances in Molecular Toxicology*, ed. J. C. Fishbein, Elsevier, 2010, vol. 4, pp. 183–222.] (-2, 0, +2 and +4) and analyzed through the calculation of intrinsic reaction coordinate paths and the application of the activation strain model. The results allow to highlight the different behavior of S, Se and Te in highly oxidizing environments.

Introduction

Sulfur and selenium are found next to each other in the periodic table and belong to group 16, i.e. the chalcogens group. Hence, they show some similarities in their chemical properties but are also strikingly different in many aspects (an interesting comparison between the properties of these two elements can be found in a paper by Wessjohan and co-workers[1]). Their biological role, for example, is quite different as sulfur is an ubiquitous element, whereas selenium is present only in a handful of compounds and is thus considered a rare biological element.[2] Moreover, sulfur has always been recognized as an essential element in biology; [3] on the other hand, selenium was first identified only as a livestock toxin,[4] and it took an extended time after its discovery before its vital role was confirmed. [5–7] Besides, human sulfur intake can reach several hundreds of mg per day without any severe consequences, whereas values of as little as 900 μg per day of selenium can have damaging effect on the human body. [8] Another important difference is found in the activity of some crucial enzymes which can express their full function only thanks to the presence of a selenium atom. The family of glutathione peroxidases (GPx) is a chief example among them, requiring in some isoforms an active selenocysteine to perform their catalytic role. [9–12] Mutations on a murine GPx, in which selenium was substituted by sulfur, showed a decrease in activity of about 1000-fold. [13,14] Theoretical studies on the catalytic site of GPx4 confirm the higher performance of selenium, compared to sulfur and tellurium, in the first mechanistic step, i.e. the reduction of the hydroperoxide. [15] However, in other enzymatic systems the substitution of selenium by sulfur hardly affected reactivity. [16] These conflicting results, combined with the fact that the insertion of a selenium atom in selenoproteins is a very complex and energy-consuming process, [17,18] raises the question why selenium is still present in biology, which remains a not fully resolved issue. [2] On another front, small models resembling the active sites of these enzymes or suitable to study elementary enzymatic steps might help to rationalize the intrinsic elemental redox properties of sulfur and selenium, [19,20] since the highly reversible redox chemistry of the latter has been recently identified as the main reason for the presence of selenium in very specific enzymes. [2,21]

One of the major roles of the antioxidant thiol-based peroxidases, containing either sulfur or selenium in the catalytic pocket, is to regulate the redox environment inside the cell, maintaining the redox signal cascade and preventing high levels of oxidative stress, which can lead to cell death. In both of these processes, hydrogen peroxide, a well-known metabolite of the normal cellular mechanism, [22] can act as a signal initiator as well as a source of free radicals that can increase the oxidative stress levels. H₂O₂ is a strong oxidant, but usually reactions involving it require a high activation barrier and are therefore kinetically slow. [22,23] However, reduction of H₂O₂ is performed with high efficiency in thiol-based enzymes such as peroxiredoxins, glutathione peroxidases and oxyR, with rate constants up to 5 x 10⁷ M⁻¹ s⁻¹, [24–26] which involve the oxidation of a chalcogen atom in this process. In the last three decades, GPx activity has inspired the synthesis of numerous organoselenides for application in human health care as antioxidants. [27–30] Among them, ebselen (2-phenyl-1,2-benzisoselenazol-3(2H)-one) [31–33] has reached the clinical trial stage, while diphenyldiselenide has been thoroughly investigated *in vitro* and *in vivo* by Rocha and coworkers [34–37] who reported on its very promising antioxidant capacity as GPx mimic. Phenylselenol, like other arylselenols, is considered an important target for chemoprevention because their metabolites have low or no toxicity. [38]

Diphenyldiselenide is largely employed also in organic catalysis, and like other selenium compounds it acts mainly as oxygen transfer agent. It is established that in most reactions the active catalyst is the benzeneperoxyseleninic acid, i.e. an oxidized form of phenylselenol. In fact, the Se-Se bond is easily cleaved in aqueous solutions of H₂O₂ and phenylselenol and its oxidized derivatives form. [39] Very recently, Back has reported that in cyclooctene epoxidations with benzeneseleninic acid (generated in situ from a diselenide precursor) the principal oxidant is presumably an thus far unknown benzeneperoxyselenonic acid. [40]

Santi focused more on the preparation of these Se based compounds reporting how many of them can be synthesized using environmentally friendly processes and thus moving towards an ever greener chemistry. [41,42]

Descending from selenium along the group 16, tellurium is encountered, which shows quite promising properties as a highly efficient antioxidant, both in small molecules [43–45] and in artificial enzymes. [46,47] However, the complete absence of a biological role for tellurium presents an obstacle to its employment *in vitro* and *in vivo*. In fact, precise and complete knowledge of the acute and long-term toxicity of tellurium compounds is needed to allow their employment in pharmacology and medicine. [27,48,49] Several research groups lean towards the idea that these compounds end up doing more harm than good, due to the very high reactivity of tellurium which acts eventually as a pro-oxidant, resulting in cell damage. [50–53] Nevertheless, substitution of selenium by tellurium in semi-artificial enzymes showed promising results [46,47] and fine-tuning of the high reactivity of organotellurides through rational molecular design might be important to synthesize effective, efficient and biologically viable molecules.

The different reactivity of sulfur, selenium and tellurium can be unraveled through modern *in silico* methodologies which offer a great opportunity to describe the fine details of chemical reactivity. State-of-the-art density functional theory (DFT) based techniques represent one of these powerful tools to accurately model chemical reactions. In this work, we present a set of *in silico* sequential oxidation reactions of phenyl-thiol, selenol and tellurol by hydrogen peroxide. Phenylthiol and phenylselenol have been chosen to compare the different reactivity of sulfur and selenium towards H_2O_2. For sake of completeness, phenyltellurol was also included. Our mechanism of choice encompasses a series of processes that starting from these reactants leads to the phenylsulfonic, phenylselenonic and phenyltelluronic acids, in a stepwise manner, spanning all the biologically relevant chalcogens oxidation states. Importantly, these species are oxidized intermediates in diphenyldiselenide catalyzed oxidations by H_2O_2. Moreover, the calculation of the intrinsic reaction coordinate (IRC) paths of selected steps and their quantitative energy decomposition through the activation strain model, [54,55] elucidates the reason behind the different activation energies needed in the processes, shedding some light on kinetic aspects. These results provide a better understanding of the chemistry of oxidized phenylchalcogenols, and more in general of the oxidations by H_2O_2 of the different chalcogen nuclei. [56]

Computational methodology

All calculations were carried out with the Amsterdam Density Functional (ADF) suite of programs. [57–59] The OLYP functional was chosen, which comprises the OPTX exchange part [60] and the Lee-Yang-Parr correlation functional, [61–63] combined with a triple-ζ quality basis set of Slater-type functions (TZ2P). The innermost orbitals of each element were kept constant during

the SCF cycles (frozen core approximation): up to 1s for carbon, nitrogen and oxygen, up to 2p for chlorine, up to 3p for selenium and up to 4p for tellurium. The scalar zeroth order regular approximation (ZORA) [64–66] was employed to account for relativistic effects. Calculations in the condensed phase were carried out in a continuum medium utilizing the Conductor-like Screening Model (COSMO)[67], as implemented in the ADF program. [68] The level of theory is therefore denoted ZORA-OLYP/TZ2P for calculations in gas phase and COSMO-ZORA-OLYP/TZ2P for calculations in the condensed phase. This level of theory was benchmarked [69] and applied with success to S_N2 mechanistic studies on organochalcogenides. [70]
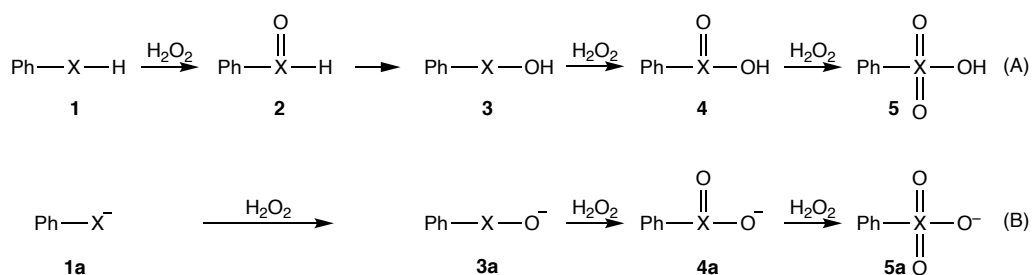
All stationary points were fully optimized and resulting geometries were confirmed with frequency calculations: minima were seen to have no imaginary frequencies, whereas transition states displayed only the imaginary frequency connected with the correct normal mode for the proceeding of the reaction. Reaction paths were calculated using the Intrinsic Reaction Coordinate (IRC) method, as implemented in ADF. [71,72] For selected reactions, the Activation Strain Model (also known as the distortion/interaction model) [54,55] was applied along the IRC path to analyze the contributions taking part in the buildup of the energetic barriers. This is a fragment-based approach that identifies two main energetic contributions to construct the total reaction energy and can be applied to a whole chemical reaction provided a suitable reaction coordinate (ξ) is selected (Equation 1):

$$\Delta E(\xi) = \Delta E(\xi)_{strain} + \Delta E(\xi)_{int} \qquad (1)$$

$\Delta E(\xi)_{strain}$ is the distortion energy needed to transform the reactant fragments from their original geometry to the one they adopt along the pathway towards products and $\Delta E(\xi)_{int}$ is the interaction energy of the reacting fragments along the chosen reaction coordinate. Calculation of the strain and interaction contributions along the reaction coordinate was carried out using PyFrag 2019. [73]

Results and discussion.

The oxidation of model phenylcalcogenols of general formula PhXH (X=S, Se and Te) by hydrogen peroxide was investigated *in silico* (Scheme 1). Two different situations were chosen, i.e. the oxidation of i) the neutral phenylchalcogenol (Scheme 1A) and ii) the anionic phenylchalcogenolate (Scheme 1B). In each consecutive step, a molecule of H_2O_2 is added that is being reduced in the process; this results in the oxidation of the chalcogen center and the displacement of a molecule of water. The only exception is the reaction that proceeds from **2** to **3,** which is a redox isomerization. In the following, the reactions will be denoted with the numbers of the two structures that represent the reactant and product separated by a dash (e.g. **2-3** for the redox isomerization reaction mentioned above).

Scheme 1 Studied reactions with the neutral phenylchalcogenol (A) and with phenylchalcogenolate (B). The water molecule formed after each oxidation is not reported for clarity. X = S, Se, Te

Oxidation of the phenylchalcogenols by H_2O_2

The sets of studied reactions comprise four steps that, starting from a compound of general formula PhXH (**1**), arrive at $PhX(O)_2OH$ (**5**), after three sequential oxidations (**1-2**, **3-4** and **4-5**) and an isomerization process (**2-3**). The mechanism of the three oxidation steps is quite similar: first, the formation of a reactant complex occurs, in which hydrogen peroxide is weakly bound to the chalcogen substrate. The reactant complex is slightly stabilized with respect to the corresponding free reactants (see SI, Table S1). Then, the elongation of the O-O bond in H_2O_2 leads to the transition state and the reaction ends with the formation of a new oxygen-chalcogen bond and the displacement of a water molecule. As example, the transition states computed for the oxidations of phenylselenol are shown in Figure 1.
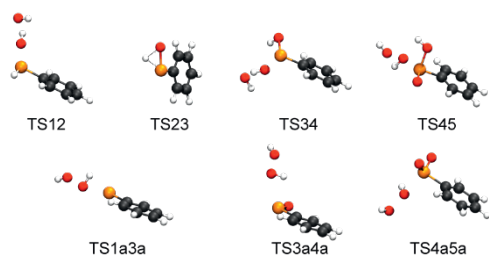

Figure 1 Transition states computed for the sequential oxidations of phenylselenol. Level of theory ZORA-OLYP/TZ2P

The calculated activation energies show that the activation barriers do not increase or decrease monotonically with the increase of the oxidation state of the chalcogen (Table 1). Most strikingly, the reactions leading to the chalcogen with a formal oxidation state of +2 (i.e. to phenylsulfinic, phenylseleninic or phenyltellurinic acids, **4**) are those with the lowest activation barrier; i.e. the reaction with the second molecule of H_2O_2 (**3-4**) is favored with respect to the first oxidation. Then, by increasing its oxidation state, the chalcogen loses part of its nucleophilic character, and therefore the last oxidation step (**4-5**) has always a higher barrier than the previous ones. Interestingly, even though the change in barrier from **1-2** to **3-4** amounts to ca. -7 kcal mol^{-1} for all three chalcogens (S, Se, Te), the increase of the last barrier (**4-5**) compared to **3-4** is far greater for tellurium compounds (20.4 kcal mol^{-1}) than for sulfur ones (6.9 kcal mol^{-1}), with selenium positioned in between (15.5 kcal mol^{-1}).

Table 1 Activation energies (kcal mol^{-1}) for the oxidation of the phenylchalcogenols by H_2O_2 (Scheme 1, Path A). Level of theory ZORA-OLYP/TZ2P.

	$\Delta E^{\ddagger}$		
	S	Se	Te
1-2	27.1	24.0	16.5
2-3	38.8	31.0	31.5
3-4	19.3	16.8	9.4
4-5	26.2	32.3	29.8

Importantly, when going from the chalcogenol form (**1**) to the sulfenic/selenenic/tellurenic state (**3**), the reaction proceeds via a chalchogenoxide (**2**) that can isomerize to form the sulfenic/selenenic/tellurenic acids. This isomerization has quite a substantial activation energy (38.8, 31.0 and 31.5 kcal mol^{-1} in the case of S, Se and Te, respectively) in the gas phase, and despite some earlier work hinting at the possibility of this activation energy to shrink in the presence of a solvent, [20] our calculations with a continuum dielectric medium solvation model have shown that this barrier slightly increases in water (see SI, Table S2). [74]

An orbital analysis of the structures found in these model reactions shows that the energy of the HOMO of the reactant is related to the energy required by the oxidations (Figure 2). The lower the energy of the HOMO of the reacting species is, the higher the activation energy is due to a less favorable interaction with the unoccupied orbitals of hydrogen peroxide. A similar behavior relating the reactivity towards H_2O_2 and HOMO energy was also found in the oxidation by H_2O_2 of dichalcogenides in a recent work by some of us. [45] Particularly, the isomerization (**2-3**) leads to **3**, whose HOMO is higher in energy than that of 1 (Figure 2). Hence, the subsequent oxidation (**3-4**) results kinetically favored with respect to reaction **1-2**. Finally, **4** has a HOMO lower in energy than either **1** or **3**, which causes the reaction (**4-5**) to have the highest barrier. Comparing the energy barriers of reaction (**1-2**) for the three different phenylchalcogenols, it is clear how tellurium oxidizes most easily with an activation energy of 16.5 kcal mol^{-1}, followed by selenium and sulfur which are more resistant to oxidation with barriers of 24.0 and 27.1 kcal mol^{-1}, respectively.
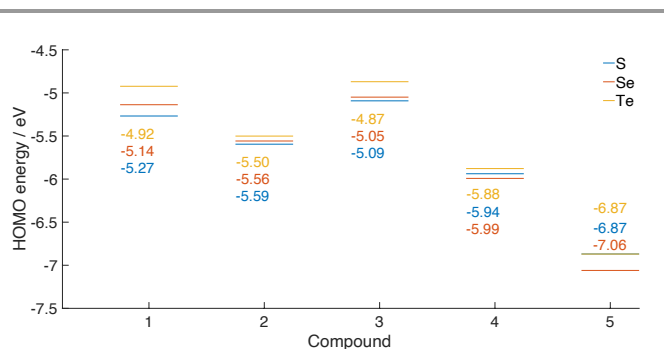
Figure 2 Energy of the HOMOs of the phenylchalcogenols and their oxidized derivatives. Level of theory ZORA-OLYP/TZ2P

The same trend is seen in reaction (**3-4**), with the transition state of the reaction with tellurium having a relative energy of 9.4 kcal mol^{-1} and those of selenium and sulfur lying 16.8 and 19.3 kcal mol^{-1} above their reactant complexes, respectively. What disrupts the behavior above described is the last oxidation (**4-5**). An analogous oxidation involving cysteine (and in a few cases selenocysteine) residues, found in many essential enzymes, is crucial in biological systems because, while reduction from the sulfinic state is still possible through the intervention of the sulfiredoxin enzyme, in case that the +4 oxidation state would be reached no mechanism is known to reduce these oxidized residues. Therefore, if they are part of the enzymatic active site, this would lead to the complete inactivation of the enzyme with consequent cellular damage. [23] Our calculations show clearly that in reaction (**4-5**) sulfur presents the lowest activation energy (26.2 kcal mol^{-1}) followed by tellurium and selenium with a barrier of 29.8 and 32.3 kcal mol^{-1}, respectively. [39] Looking in more detail at the orbital structures of **1**, **3** and **4**, we can see that when comparing analogous structures (*i.e.* either **1**, **3** or **4**) containing different chalcogens, the energies of the HOMO orbitals of the reactants mirror the trend found for activation energies (Figure 2), meaning that a substrate with a lower HOMO is expected to have a less favorable activation energy. This is confirmed by our calculations which for **1** and **3** show that the HOMO energy is decreasing when going from tellurium to sulfur and holds true also for the last oxidation in which the order of the activation energies changes as compound **4** shows HOMOs of progressively descending energy in the order tellurium, sulfur and lastly selenium.

We have further analyzed this last oxidation step applying the activation strain model to the reaction. As a suitable reaction coordinate, we chose the O-O distance in hydrogen peroxide relative to that measured in the relaxed H_2O_2 molecule (which at ZORA-OLYP/TZ2P level of theory is 1.46 Å). Since we are interested in the causes underlying the formation of the energy barriers, the reaction path was modelled leading up to the transition state, disregarding the second half of the reaction leading to the products (Figure 3).

The analysis of the energy contributions to the total (relative) reaction energies for reaction (**4-5**) with the three different chalcogens shows how the strain and the interaction contributions play their part in determining the height of the

barriers. Although the reaction coordinate was chosen to be independent from the chalcogen, the activation strain analysis performed along the reaction coordinate, highlights how the transition states are reached at different values of it. Sulfur has the earliest transition state at a ξ_{TS} value of 0.53 Å followed by selenium (ξ_{TS}=0.55 Å) and lastly tellurium (ξ_{TS}=0.57). However, as previously mentioned, the energies of the transition states are not related to the value of their reaction coordinate since in presence of selenium the reaction has the highest barrier. The strain energy is computed to be quite similar for the three cases, albeit in the last part of the reaction a sharp increase of this contribution is seen in the presence of selenium. The curves of the interaction energy almost overlap in the presence of sulfur and tellurium throughout the whole path to the transition state, whereas, in the case of selenium, the curve is higher. This smaller stabilizing interaction is ultimately the reason for the higher barrier found in the last oxidation of the selenium compound. [75]
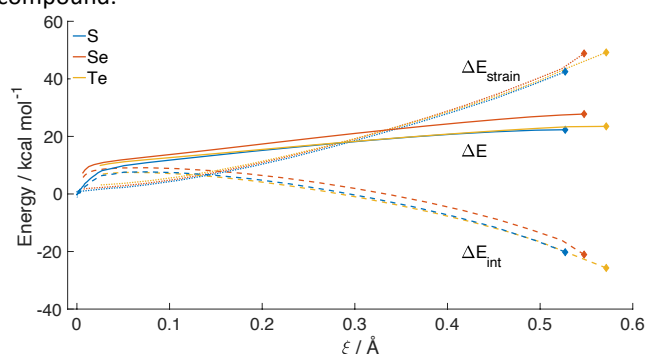

Figure 3 Activation strain analysis of reaction (**4-5**). The diamonds represent the transition states. Level of theory ZORA-OLYP/TZ2P.

Oxidation of the phenylchalcogenolates by H_2O_2

We have investigated the analogous series of reactions using phenylchalcogenolate anions (Scheme 1B), in which the nucleophilic strength of sulfur/selenium/tellurium is certainly enhanced. Owing to the absence of the proton involved in the isomerization from **2** to **3**, this mechanistic path consists of three sequential oxidations. The optimized reactant complexes for all the reactions show a much stronger stabilization than those of path A (see SI, Table S3) and also the transition states are located at lower energies than the free reactants.

The presence of the negative charge on the chalcogenolate changes the picture quite dramatically. First, all reactions become more favored as the nucleophilic character of the chalcogen atom is definitively increased by the presence of the negative charge (Table 2). Moreover, sulfur behaves differently from its siblings: its first oxidation (**1a-3a**) has a barrier of 12.2 kcal mol^{-1} which slightly decreases in the subsequent step (**3a-4a**, 11.2 kcal mol^{-1}) and is identical to that computed for the final oxidation (**4a-5a**). On the other hand, the activation energy for selenium and tellurium compounds is found to increase with the oxidation state of the chalcogen. Reaction **1a-3a** shows the lowest barrier for both chalcogens (10.2 and 8.2 kcal mol^{-1} for

selenium and tellurium, respectively), which then increases for both subsequent oxidation steps.

Comparing the same step with different chalcogens, we see that the first reaction (**1a-3a**) is kinetically more favored as we move from sulfur ($\Delta E^{\ddagger}$=12.3 kcal mol^{-1}) down group 16 to selenium ($\Delta E^{\ddagger}$=10.2 kcal mol^{-1}) and tellurium ($\Delta E^{\ddagger}$=8.2 kcal mol^{-1}).

Table 2 Activation energies (kcal mol^{-1}) for the oxidation of the phenylchalcogenolates by H_2O_2 (Scheme 1, Path B). Values in parentheses in italics are computed in water. Level of theory (COSMO)-ZORA-OLYP/TZ2P.

	$\Delta E^{\ddagger}$					
	S		Se		Te	
1a-3a	12.3	*(7.4)*	10.2	*(5.5)*	8.2	*(3.7)*
3a-4a	11.2	*(8.4)*	12.0	*(9.4)*	12.0	*(8.9)*
4a-5a	11.2	*(10.0)*	16.5	*(16.2)*	16.8	*(16.4)*

The subsequent oxidations are instead easier for sulfur compounds, albeit differences are quite small (less than 1 kcal mol^{-1}). An interesting thing to note is that for the last two reactions involving selenium or tellurium the activation energies are almost identical, meaning that the reactivity of the oxidized form of these chalcogenolates is very similar.

The energy profile of reaction (**4a-5a**) was calculated through IRCs from each reactant complex to the corresponding transition state. For consistency with the previously calculated IRCs, the reaction coordinate (ξ) was chosen to be the O-O distance in H_2O_2 relative to the distance in the optimized hydrogen peroxide molecule. The total energy was then decomposed into $\Delta E(\xi)_{strain}$ and $\Delta E(\xi)_{int}$. (Figure 4)

The obtained reaction profiles are quite different from those of reaction (**4-5**). Both strain and interaction contributions are found to be, in absolute value, smaller than in the neutral reactions and transitions states occur at earlier ξ values. Moreover, although the reaction coordinate was chosen not to involve directly the chalcogen atom, the transition states are found at different positions along the IRC profile: sulfur has the earliest transition state, with a ξ value of 0.22 Å followed by tellurium (ξ=0.28 Å) and selenium (ξ=0.38 Å). The decomposition of the reaction energies shows that the strain contributions are almost equal for all three chalcogenolates and the differences in the total energy mainly arise from the interaction part. In particular, this is more evident in the case of sulfur which shows the most favorable interaction, resulting in an overall more stabilized reaction profile and in a lower activation barrier. On the other hand, in the cases of selenium and tellurium very similar reaction profiles are observed with the only noticeable difference in the very beginning of the reaction where in the case of Te a slightly more positive interaction energy and thus an overall higher energy are computed. To clarify the reason why sulfur has a more stabilizing interaction contribution we decomposed the interaction energy and saw that this effect arises because of the smaller inter-electronic repulsion that acts on the sulfur species (i.e. a smaller ΔE_{Pauli}, see figure S2). In fact, the other contributions that give the total interaction, electrostatic

interaction (ΔV_{Elstat}) and orbital interaction (ΔE_{OI}) were found to be very similar after the very beginning of the reaction (see Figure S2).
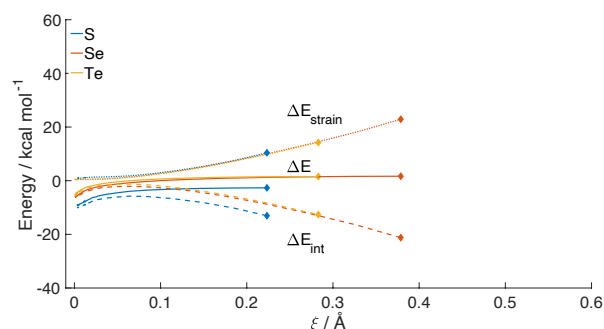

Figure 4 Activation strain analysis of reaction (**4a-5a**). The diamonds represent the transition states. Level of theory ZORA-OLYP/TZ2P.

Finally, we modelled Path B in presence of solvent. We employed a continuum solvation method (COSMO) using the parameters for water. Starting from the gas phase structures, full optimization of all the stationary points in water resulted in very similar structures, proving that no change of mechanism is expected in condensed phase. The computed energies show that in the condensed phase the activation barriers of all the reactions diminish (Table 2). The effect is strongest for the first oxidation (**1a-3a**) and disappears as we proceed along the reaction pathway. A justification to this behavior can be traced to the more favorable solvation energies calculated for the transition states than for the weakly bound reactant complexes directly preceding them (see SI, Table S4). This is most probably due to the fact that, moving from the reactant complex to the transition state, part of the charge, which is initially present on the chalcogen atom, is transferred to an oxygen atom, resulting in a situation where the charge accumulates on a smaller atom (O). This localization of charge at the TS translates into a more favorable solvation energy in presence of a polar solvent (water); this effect was already reported for a series of anionic bases in water,[76] but there the situation was reversed (the reactants has larger charge localization, leading to an increase of the barriers). Moreover, sulfur is the chalcogen that most benefits from solvation, which is again in agreement with the fact that S is the smaller chalcogen, giving rise to a stronger localization of the negative charge. Looking at the activation energies of the reactions in water, we can see that in the cases of selenium and tellurium smaller activation barriers for the first oxidation (**1a-3a**) are observed than in presence of sulfur. But in all three cases similar barriers (within 1 kcal mol^{-1}) are computed for the second oxidation (**3a-4a**) and in the last step (**4a-5a**) the trend is reversed, as the reaction becomes less kinetically favored when moving down the group.

Conclusions

This work presents an *in silico* study on the oxidation by H_2O_2 of model phenylchalcogenols PhXH (**1**) or their deprotonated form PhX$^-$ (**1a**) (X=S, Se or Te). A stepwise mechanistic path that leads from PhXH/PhX$^-$ to the fully oxidized PhXO$_3$H (**5**)/PhXO$_3^-$ (**5a**)

was investigated with a relativistic DFT approach. IRC energy profiles were calculated and decomposed along the reaction coordinate, employing the activation strain model, for one selected elementary step.

When starting from compound **1** (Path A), the mechanism consists of four reactions: three of them being red-ox steps (**1-2**, **3-4** and **4-5**) and one an isomerization process (**2-3**). Analyzing the oxidation steps, we found that, in presence of sulfur, selenium or tellurium, the barrier encountered in the first oxidation (**1-2**) decreases in the second oxidative process (**3-4**) due to the presence of the intermediate isomerization reaction (**2-3**) that transforms the PhX(O)H compound into a sulfenic/selenenic/tellurenic acid which is more reactive towards H_2O_2 than the starting thiol/selenol/tellurol. The final step (**4-5**) shows a systematically higher barrier than the preceding one (**3-4**), caused by the loss of nucleophilic character of the chalcogen atom due to the presence of the electron withdrawing oxygen atoms. Importantly, considering the whole process, the isomerization reaction is the step with the highest barrier in the case of sulfur and tellurium and it is very close to the highest barrier for the mechanism involving selenium. Moreover, inclusion of a continuum dielectric in this step does not cause the barrier of reaction (**2-3**) to shrink in presence of any chalcogen. When comparing the reactivity of the different chalcogens in the same reaction, we found that for the first two oxidations the activation energy increases going from tellurium to selenium and sulfur. On the other hand, in reaction (**4-5**) selenium is predicted to be the most difficult to oxidize, followed by tellurium and lastly sulfur. Decomposition of the bonding energy along the chosen reaction coordinate (the O-O distance in H_2O_2) shows that the reason underlying the resistance to oxidation of selenium in reaction (**4-5**) can be directly found in the weaker ΔE_{int} contribution throughout the process.

Regarding the mechanistic path starting from **1a** (Path B), strong similarities are found, with the only difference that no isomerization reaction is needed, owing to the absence of the proton that is transferred. The behavior observed along the whole sequence of oxidations differs in the case of sulfur. For the lightest chalcogen, the reaction barriers are seen to be almost equal for the three oxidation steps (with a slight decrease going from reaction **1a-3a** to reaction **3a-4a**), whereas an appreciable increase in the activation energies is observed in presence of selenium and tellurium when going towards higher oxidation states. Comparing the reactivity of the three chalcogenolates, we found that in the first oxidation there is an increase in the activation energy going from tellurium to sulfur, whereas for the subsequent reactions tellurium and selenium show similar barriers that are overall higher than those of sulfur. Decomposition of the energy profile of the reaction (**4a-5a**) points out that different interaction contributions determine the different reactivity in the case of sulfur with respect to the cases of selenium and tellurium.

When modelling path B in water (included through a dielectric continuum model), an analogous mechanism was found with a diminution of all reaction barriers. This effect can be ascribed to the greater solvation energies calculated for the transition states than for the reactant complexes, in all cases, due to a stronger charge localization taking place at the TS.

These results sketch a well-defined picture of the reactivity of phenylchalcogenols toward H_2O_2. Our calculations reveal that, if selenium and tellurium are easier to oxidize than sulfur when they are in their lower oxidation states, as the process continues, leading towards higher oxidation states, they become more resistant to oxidation than sulfur. This is true for reaction involving neutral and anionic chalcogen species, both *in vacuo* and in water. This peculiar feature could be a key point to explain why selenium is present instead of sulfur in some biological systems found in highly oxidizing environments and is certainly an advantageous trait that could be exploited in the rational design of systems containing selenium and tellurium mimicking a precise biologically relevant redox function, which could potentially outperform their sulfur analogues. However, for this last ambitious step, further experimental investigation is prompted on the *in vivo* reactivity of these compounds and their biocompatibility (especially in the case of tellurium).

Conflicts of interest

There are no conflicts to declare.

Acknowledgements

Author information

Marco Bortoli, ORCID 0000-0001-5506-6347
Matteo Bruschi, ORCID 0000-0001-7838-0363
Marcel Swart, ORCID 0000-0002-8174-8488
Laura Orian, ORCID 0000-0002-1673-5111

Notes and references

1   L. A. Wessjohann, A. Schneider, M. Abbas and W. Brandt, *Biol. Chem.*, 2007, **388**, 997–1006.

2   H. J. Reich and R. J. Hondal, *ACS Chem. Biol.*, 2016, **11**, 821–841.

3   In *Van Nostrand's Scientific Encyclopedia*, John Wiley & Sons, Inc., Hoboken, NJ, USA, 2005.

4   K. W. Franke, *J. Nutr.*, 1934, **8**, 597.

5   J. Pinsent, *Biochem. J.*, 1954, **57**, 10–16.

6   E. L. Patterson, R. Milstrey and E. L. R. Stokstad, *Exp. Biol. Med.*, 1957, **95**, 617–620.

7   K. Schwarz and C. M. Foltz, *J. Am. Chem. Soc.*, 1957, **79**, 3292–3293.

8   World Health Organization, *Guidelines for drinking-water quality: fourth edition incorporating the first addendum.*, World Health Organization, Geneva, 2017.

9   F. Ursini, M. Maiorino and C. Gregolin, *BBA - Gen. Subj.*, 1985, **839**, 62–70.

10   S. Toppo, L. Flohé, F. Ursini, S. Vanin and M. Maiorino, *Biochim. Biophys. Acta - Gen. Subj.*, 2009, **1790**, 1486–1500.

11   R. Brigelius-flohé and M. Maiorino, *BBA - Gen. Subj.*, 2013, **1830**, 3289–3303.

12   L. Orian, G. Cozza, M. Maiorino, S. Toppo and F. Ursini, in *Glutathione*, ed. L. Flohé, CRC Press, 2018, pp. 53–66.

13   C. Rocher, J.-L. Lalanne and J. Chaudiére, *Eur. J. Biochem.*, 1992, **205**, 955–960.

14   M. Maiorino, V. Bosello-Travain, G. Cozza, G. Miotto, L. Orian, A. Roveri, S. Toppo, M. Zaccarin and F. Ursini, in *Selenium: Its Molecular Biology and Role in Human Health, Fourth Edition*, eds. D. L. Hatfield, U. Schweizer, P. A. Tsuji and V. N. Gladyshev, Springer International Publishing, 2016, pp. 223–234.

15   M. Bortoli, M. Torsello, F. M. Bickelhaupt and L. Orian, *ChemPhysChem*, 2017, **18**, 2990–2998.

16   S. M. Kanzok, A. Fechner, H. Bauer, J. K. Ulschmid, H. M. Müller, J. Botella-Munoz, S. Schneuwly, R. H. Schirmer and K. Becker, *Science* , 2001, **291**, 643–646.

17   K. Forchhammer, W. Leinfelder and A. Böck, *Nature*, 1989, **342**, 453–456.

18   J. Heider, C. Baron and A. Böck, *EMBO J.*, 1992, **11**, 3759–3766.

19   B. Cardey and M. Enescu, *J. Phys. Chem. A*, 2007, **111**, 673–678.

20   L. A. H. van Bergen, G. Roos and F. De Proft, *J. Phys. Chem. A*, 2014, **118**, 6078–6084.

21   R. J. Hondal and E. L. Ruggles, *Amino Acids*, 2011, **41**, 73–89.

22   C. C. Winterbourn, in *Methods in Enzymology*, Academic Press, 2013, vol. 528, pp. 3–25.

23   P. Nagy and C. C. Winterbourn, in *Advances in Molecular Toxicology*, ed. J. C. Fishbein, Elsevier, 2010, vol. 4, pp. 183–222.

24   A. Perkins, K. J. Nelson, D. Parsonage, L. B. Poole and P. A. Karplus, *Trends Biochem. Sci.*, 2015, **40**, 435–445.

25   L. Orian, P. Mauri, A. Roveri, S. Toppo, L. Benazzi, V. Bosello-Travain, A. De Palma, M. Maiorino, G. Miotto, M. Zaccarin, A. Polimeno, L. Flohé and F. Ursini, *Free Radic. Biol. Med.*, 2015, **87**, 1–14.

26   I. Jo, I.-Y. Chung, H.-W. Bae, J.-S. Kim, S. Song, Y.-H. Cho and N.-C. Ha, *Proc. Natl. Acad. Sci. U. S. A.*, 2015, **112**, 6443–8.

27   C. W. Nogueira, G. Zeni and J. B. T. T. Rocha, *Chem. Rev.*, 2004, **104**, 6255–6285.

28   K. P. Bhabak and G. Mugesh, *Acc. Chem. Res.*, 2010, **43**, 1408–1419.

29   L. Orian and S. Toppo, *Free Radic. Biol. Med.*, 2014, **66**, 65–74.

30   M. Dalla Tiezza, G. Ribaudo and L. Orian, *Curr. Org. Chem.*, 2018, 22, 1–21.

31   A. Wendel, M. Fausel, H. Safayhi, G. Tiegs and R. Otter, *Biochem. Pharmacol.*, 1984, **33**, 3241–3245.

32   A. Müller, E. Cadenas, P. Graf and H. Sies, *Biochem. Pharmacol.*, 1984, **33**, 3235–3239.

33   M. J. Parnham and H. Sies, *Biochem. Pharmacol.*, 2013, 86, 1248–1253.

34   W. Hassan and J. Rocha, *Molecules*, 2012, **17**, 12287–12296.

35   J. T. Da Rocha, A. Sperança, C. W. Nogueira and G. Zeni, *J. Pharm. Pharmacol.*, 2009, **61**, 1673–1679.

36   A. F. De Bem, B. Fiuza, P. Calcerrada, P. M. Brito, G. Peluffo, T. C. P. Dinis, M. Trujillo, J. B. T. Rocha, R. Radi and L. M. Almeida, *Nitric Oxide - Biol. Chem.*, 2013, **31**, 20–30.

37   A. S. De Freitas and J. B. T. Rocha, *Neurosci. Lett.*, 2011, **503**, 1–5.

38   H. E. Ganther and J. R. Lawrence, *Tetrahedron*, 1997, **53**, 12299–12310.

39   G. Ribaudo, M. Bellanda, I. Menegazzo, L. P. Wolters, M. Bortoli, G. Ferrer-Sueta, G. Zagotto and L. Orian, *Chem. - Eur. J.*, 2017, **23**, 2405–2422.

40   K. N. Sands, E. Mendoza Rengifo, G. N. George, I. J. Pickering, B. S. Gelfand and T. G. Back, *Angew. Chemie - Int. Ed.*, , DOI:10.1002/anie.201913566.

41   S. Santoro, J. B. Azeredo, V. Nascimento, L. Sancineto, A. L. Braga and C. Santi, *RSC Adv.*, 2014, **4**, 31521–31535.

42   C. Santi, A. Zając, A. L. Braga, B. Movassag, C. Tidei, C. Santi, T. Cristina, B. Desirèe, D. Pietrella, F. Marini, F. Galli, M. Giuseppe, J. Ścianowski, J. Lewkowski, J. Drabowicz, L. Bagnoli, P. Marta, M. Iwaoka, M. Navidi, O. E. D. Rodrigues, P. Pokora-Sobczak, P. Kiełbasiński, R. S. Schwab, S. Hayashi, C. Silvia, S. Sternativo, T. Murai, W. Nakanishi and Z. Rafiński, *Organoselenium Chemistry: Between Synthesis and Biochemistry*, 2014.

43   S. P. Collins, G. S. Heverly-Coulson and R. J. Boyd, *Comput. Theor. Chem.*, 2012, **981**, 68–72.

44   M. Ibrahim, W. Hassan, D. F. Meinerz, M. dos Santos, C. V. Klimaczewski, A. M. Deobald, M. S. Costa, C. W. Nogueira, N. B. V Barbosa and J. B. T. Rocha, *Mol. Cell. Biochem.*, 2012, **371**, 97–104.

45   M. Bortoli, F. Zaccaria, M. Dalla Tiezza, M. Bruschi, C. Fonseca Guerra, F. M. Bickelhaupt and L. Orian, *Phys.*

Chem. Chem. Phys., 2018, **20**, 20874–20885.

46   S. Mao, Z. Dong, J. Liu, X. Li, X. Liu, G. Luo and J. Shen, *J. Am. Chem. Soc.*, 2005, **127**, 11588–11589.

47   X. Liu, L. A. Silks, C. Liu, M. Ollivault-Shiflett, X. Huang, J. Li, G. Luo, Y. M. Hou, J. Liu and J. Shen, *Angew. Chemie - Int. Ed.*, 2009, **48**, 2020–2023.

48   L. Tiano, D. Fedeli, A. M. Santroni, M. Villarini, L. Engman and G. Falcioni, *Mutat. Res. Toxicol. Environ. Mutagen.*, 2000, **464**, 269–277.

49   D. B. Santos, V. P. P. Schiar, M. W. Paixão, D. F. Meinerz, C. W. Nogueira, M. Aschner, J. B. T. Rocha and N. B. V. Barbosa, *Toxicol. Vitr.*, 2009, **23**, 1195–1204.

50   C. Funchal, R. B. de Andrade, E. Turcatel, R. B. Guerra, C. M. D. Wannmacher and R. Gomez, *Int. J. Dev. Neurosci.*, 2011, **29**, 903–907.

51   P. Vij and D. Hardej, *Environ. Toxicol. Pharmacol.*, 2012, **34**, 768–782.

52   D. F. Meinerz, J. Allebrandt, D. O. Mariano, E. P. Waczuk, F. A. Soares, W. Hassan and J. B. T. Rocha, *PeerJ*, 2014, **2**, e290.

53   P. Vij and D. Hardej, *Environ. Toxicol. Pharmacol.*, 2016, **43**, 216–224.

54   F. M. Bickelhaupt and E. J. Baerends, in *Reviews in Computational Chemistry*, eds. K. B. Lipkovitz and D. B. Boyd, Wiley-VCH, New York, 2000, vol. 15, pp. 1–86.

55   F. M. Bickelhaupt and K. N. Houk, *Angew. Chemie - Int. Ed.*, 2017, **56**, 10070–10086.

56   The oxidation path of organoselenides is rather complex and involves many different steps and intermediates. In this work, we have chosen the straightest path, directly connecting the sulfoxide/selenoxide/telluroxide, sulfenic/selenenic/tellurenic, sulfinic/seleninic/tellurinic and sulfonic/selenonic/telluronic forms. A more complete description is given in Scheme S1, in which peroxysulfinic/seleninic/tellurinic acid, peroxysulfonic/selenonic/telluronic and the elusive hydroxyperhydroxysulfane/selenane/tellurane are included.

57   G. te Velde, F. M. Bickelhaupt, E. J. Baerends, C. Fonseca Guerra, S. J. A. van Gisbergen, J. G. Snijders and T. Ziegler, *J. Comput. Chem.*, 2001, **22**, 931–967.

58   C. Fonseca Guerra, J. G. Snijders, G. te Velde and E. J. Baerends, *Theor. Chem. Acc.*, 1998, **99**, 391–403.

59   E. J. Baerends, T. Ziegler, A. J. Atkins, J. Autschbach, D. Bashford, O. Baseggio, A. Bérces, F. M. Bickelhaupt, C. Bo, P. M. Boerritger, L. Cavallo, C. Daul, D. P. Chong, D. V Chulhai, L. Deng, R. M. Dickson, J. M. Dieterich, D. E. Ellis, M. van Faassen, A. Ghysels, A. Giammona, S. J. A. van Gisbergen, A. Goez, A. W. Götz, S. Gusarov, F. E. Harris, P. van den Hoek, Z. Hu, C. R. Jacob, H. Jacobsen, L. Jensen, L. Joubert, J. W. Kaminski, G. van Kessel, C. König, F. Kootstra, A. Kovalenko, M. Krykunov, E. van Lenthe, D. A. McCormack, A. Michalak, M. Mitoraj, S. M. Morton, J. Neugebauer, V. P. Nicu, L. Noodleman, V. P. Osinga, S. Patchkovskii, M. Pavanello, C. A. Peeples, P. H. T. Philipsen, D. Post, C. C. Pye, H. Ramanantoanina, P. Ramos, W. Ravenek, J. I. Rodríguez, P. Ros, R. Rüger, P. R. T. Schipper,

D. Schlüns, H. van Schoot, G. Schreckenbach, J. S. Seldenthuis, M. Seth, J. G. Snijders, M. Solà, S. M., M. Swart, D. Swerhone, G. te Velde, V. Tognetti, P. Vernooijs, L. Versluis, L. Visscher, O. Visser, F. Wang, T. A. Wesolowski, E. M. van Wezenbeek, G. Wiesenekker, S. K. Wolff, T. K. Woo and A. L. Yakovlev, *ADF2018*, SCM, Theoretical Chemistry, Vrije Universiteit, Amsterdam, The Netherlands.

60   N. C. Handy and A. J. Cohen, *Mol. Phys.*, 2001, **99**, 403–412.

61   C. Lee, W. Yang and R. G. Parr, *Phys. Rev. B*, 1988, **37**, 785–789.

62   B. G. Johnson, P. M. W. Gill and J. A. Pople, *J. Chem. Phys.*, 1993, **98**, 5612–5626.

63   T. V. Russo, R. L. Martin and P. J. Hay, *J. Chem. Phys.*, 1994, **101**, 7729–7737.

64   E. van Lenthe, E. J. Baerends and J. G. Snijders, *J. Chem. Phys.*, 1993, **99**, 4597–4610.

65   R. Van Leeuwen, E. Van Lenthe, E. J. Baerends and J. G. Snijders, *J. Chem. Phys.*, 1994, **101**, 1272–1281.

66   E. Van Lenthe, *J. Chem. Phys.*, 1999, **110**, 8943–8953.

67   A. Klamt, *J. Phys. Chem.*, 1995, **99**, 2224–2235.

68   C. C. Pye and T. Ziegler, *Theor. Chem. Acc.*, 1999, **101**, 396–408.

69   F. Zaccaria, L. P. Wolters, C. C. Fonseca Guerra and L. Orian, *J. Comput. Chem.*, 2016, **37**, 1672–1680.

70   M. Bortoli, L. P. Wolters, L. Orian and F. M. Bickelhaupt, *J. Chem. Theory Comput.*, 2016, **12**, 2752–2761.

71   L. Deng, T. Ziegler and L. Fan, *J. Chem. Phys.*, 1993, **99**, 3823–3835.

72   L. Deng and T. Ziegler, *Int. J. Quantum Chem.*, 1994, **52**, 731–765.

73   X. Sun, T. M. Soini, J. Poater, T. A. Hamlin and F. M. Bickelhaupt, *J. Comput. Chem.*, 2019, **40**, jcc.25871.

74   The computed activation energies might be lowered by using explicit water molecules that mediate the proton transfer necessary for the formation of water at each oxidation step. For example, in a study on the GPx mimic behavior of phenylchalcogenol, Bayse introduces two water molecules which efficiently reduce the oxidation barrier of the compound by CH_3OOH, which is $\Delta H=12.1$ and $\Delta G=19.1$.[*J Phys Chem A*, 2007, **111**, 9070-9075] In this case, the mechanism is also different because the product is directly the selenenic acid.

75   This resistance of selenium to oxidation is analogous to the high instability of BrO_4^- vs ClO_4^- and IO_4^- (reduction potentials of the couples XO_4^-/XO_4^- 1.74 (X=Br), 1.19 (X=Cl) and 1.65 eV (X=I)) which is ascribed to the enhanced inert pair effect, that is to the outermost s-atomic orbitals which are difficult to ionize.

76   M. Swart, E. Rösler and F. M. Bickelhaupt, *Eur. J. Inorg. Chem.*, 2007, **2007**, 3646–3654.